Neutron star mass formula with nuclear saturation parameters

Hajime Sotani[1,2,*] and Hajime Togashi[3]

[1]*Astrophysical Big Bang Laboratory, RIKEN, Saitama 351-0198, Japan*
[2]*Interdisciplinary Theoretical and Mathematical Science Program (iTHEMS), RIKEN, Saitama 351-0198, Japan*
[3]*Department of Physics, Tohoku University, Sendai 980-8578, Japan*

(Received 30 December 2021; accepted 13 February 2022; published 14 March 2022)

We derive the empirical formulas for the neutron star mass and gravitational redshift as a function of the central density and specific combination of the nuclear saturation parameters, which are applicable to the stellar models constructed with the central density up to threefold nuclear saturation density. Combining both empirical formulas, one also estimates the neutron star radius. In practice, we find that the neutron star mass (radius) can be estimated within ∼10% (a few percent) accuracy by comparing the mass and radius evaluated with our empirical formulas to those determined with the specific equation of state. Since our empirical formulas directly connect the neutron star mass and radius to the nuclear saturation parameters, one can discuss the neutron star properties with the specific values of nuclear saturation parameters constrained via nuclear experiments.

DOI: 10.1103/PhysRevD.105.063010

I. INTRODUCTION

A neutron star is produced as a compact remnant through a supernova explosion, which occurs at the last moment of a massive star's life. The neutron stars are in extreme states, which is hard to be realized in terrestrial laboratories. In particular, due to the nature of the nuclear saturation properties, it is quite difficult to obtain the nuclear information in a higher density region through the terrestrial experiments. This is a reason why the equation of state (EOS) for neutron star matter has not been fixed yet. Namely, the structure of the neutron star and its maximum mass are not exactly determined. Thus, the observations of the neutron stars and/or the phenomena associated with the neutron stars are quite important for understanding the physics in such extreme states.

For example, the discovery of the $2\,M_\odot$ neutron stars [1–4] has ruled out some of the soft EOSs as the EOS for neutron star matter. That is, the EOS, with which the maximum mass does not reach the observed mass, can be ruled out. In addition, the light bending induced by the strong gravitational field, which is one of the important relativistic effects, modifies the pulsar light curve, which principally tells us the stellar compactness, i.e., the ratio of the stellar mass to its radius (e.g., [5–10]). In practice, through the observations with the Neutron Star Interior Composition Explorer operating on the International Space Station, the mass and radius of PSR J0030 + 0451 [11,12] and PSR J0740 + 6620 [13,14] are constrained. Owing to the gravitational wave observations in the event of GW170817 [15], the tidal deformability of the neutron star just before the merger of the binary neutron stars is also constrained, which tells us that the $1.4\,M_\odot$ neutron star radius should be less than 13.6 km [16]. Furthermore, it is proposed that the neutron star mass and radius may be determined with the technique of asteroseismology through the future gravitational wave observations (e.g., [17–25]). These astronomical constraints on the neutron star mass and radius indirectly constrain the EOS for neutron star matter, especially for a higher density region.

On the other hand, terrestrial experiments are obviously important for extracting the nuclear information, which also constrains the EOS for neutron star matter, even though the resultant constraint may be mainly around the nuclear saturation density. Up to now a lot of experiments worldwide have been done to fix the nuclear saturation parameters. Owing to these attempts, some of the saturation parameters have been constrained well, but many parameters, especially for higher order terms, still remain uncertain (see Sec. II for more detail). For instance, even the constraint on the density dependence of the nuclear symmetry energy, which was recently reported from two large facilities in Japan and the U.S., still has large uncertainties [26,27]. Additionally, since the EOS for neutron star matter can be characterized by the nuclear saturation parameters, the neutron star properties may be also associated with the saturation parameters. Thus, to improve our understanding of the nuclear properties, the constraint on the neutron star mass and radius from the astronomical observations are quite important as well as

*sotani@yukawa.kyoto-u.ac.jp

constraints on the nuclear properties from the terrestrial experiments.

Nevertheless, even if one would accurately observe the neutron star mass and/or radius, it is difficult to directly discuss the nuclear saturation parameters. This is because the neutron star properties are associated with the EOSs, which can be characterized by the nuclear saturation parameters, but direct connection between the neutron star properties and nuclear saturation parameters is still unclear. To partially solve this difficulty, we have already found a suitable combination of the nuclear saturation parameters, with which the low-mass neutron star models can be expressed well [28]. In this study, we extend the previous work and try to derive the empirical formulas for the mass and gravitational redshift of neutron star models constructed with the central density up to threefold nuclear saturation density, which helps us to directly discuss the association between the neutron star properties and nuclear saturation parameters.

This manuscript is organized as follows. In Sec. II, we briefly mention the EOSs considered in this study. In Sec. III, we systematically examine the neutron star models and derive the empirical formulas for the neutron star mass and its gravitational redshift as a function of the nuclear saturation parameters. Finally, in Sec. IV, we conclude this study. Unless otherwise mentioned, we adopt geometric units in the following, $c = G = 1$, where c and G denote the speed of light and the gravitational constant, respectively.

II. EOS FOR NEUTRON STAR MATTER

To construct the neutron star models by solving the Tolman-Oppenheimer-Volkoff (TOV) equation, one has to assume an EOS for neutron star matter. In this study, we mainly adopt the phenomenological nuclear EOS models, focusing only on the unified EOS, i.e., the neutron star crust EOS is constructed with the same nuclear model as in the neutron star core EOS. As a phenomenological macroscopic model, we adopt the EOSs proposed by Oyamatsu and Iida (hereafter referred to as the OI-EOS) [29,30]. The OI-EOSs are constructed with the Padé-type potential energies in such a way as to reproduce empirical masses and radii of stable nuclei, using a simplified version of the extended Thomas-Fermi theory. On the other hand, as a phenomenological Skyrme-type model, we adopt KDE0v, KDE0v1 [31], SLy2, SLy4, SLy9 [32,33], SKa [34], SkI3 [35], and SkMp [36]. In addition, we also adopt the Shen EOS [37], which is based on the relativistic mean field theory, and the Togashi EOS [38], which is derived by the variational many-body calculation with AV18 two-body and UIX three-body potentials. In Fig. 1, we show the mass and radius relation for the neutron star models constructed with the EOSs adopted in this study, where the stellar models with $n_c/n_0 = 1$, 2, and 3 are shown with the marks. We note that some of the stellar models with $n_c/n_0 = 1$ are out of the panel due to the large radius. One can observe

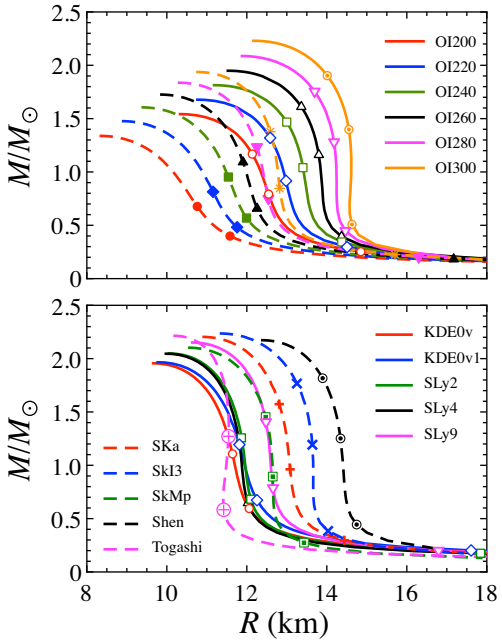

FIG. 1. Mass and radius relation for the neutron star models constructed with the EOSs listed in Table I, where the top and bottom panels correspond to the result with OI-EOSs and the others, respectively. The OI-EOSs are named with the value of K_0, e.g., OI200 for the OI-EOSs with $K_0 = 200$ MeV. Top: the solid and dashed lines, respectively, denote the OI-EOSs with larger and smaller values of L for each value of K_0 (see Table I). In each panel, the neutron star models with $n_c/n_0 = 1$, 2, and 3 are shown with the marks.

that some of EOSs are obviously ruled out from the $2\,M_\odot$ observations [1–4] or the radius constraint from the GW170817 [16], but in order to examine with the wide parameter space, we adopt even such EOSs in this study.

In any case, the bulk energy per nucleon for the uniform nuclear matter at zero temperature can generally be expressed as a function of the baryon number density $n_\mathrm{b} = n_n + n_p$ and an asymmetry parameter $\alpha = (n_n - n_p)/n_\mathrm{b}$, with the neutron number density n_n and the proton number density n_p,

$$\frac{E}{A} = w_s(n_\mathrm{b}) + \alpha^2 S(n_\mathrm{b}) + \mathcal{O}(\alpha^3), \tag{1}$$

where w_s corresponds to the energy per nucleon of symmetric nuclear matter, while S denotes the density-dependent symmetry energy. Additionally, w_s and S can be expanded around the saturation density n_0 of the symmetric nuclear matter as a function of $u = (n_\mathrm{b} - n_0)/(3n_0)$,

$$w_s(n_\mathrm{b}) = w_0 + \frac{K_0}{2}u^2 + \frac{Q}{6}u^3 + \mathcal{O}(u^4), \tag{2}$$

$$S(n_\mathrm{b}) = S_0 + Lu + \frac{K_\mathrm{sym}}{2}u^2 + \frac{Q_\mathrm{sym}}{6}u^3 + \mathcal{O}(u^4). \tag{3}$$

TABLE I. EOS parameters adopted in this study, K_0, n_0, L, Q, $K_{\rm sym}$, and $Q_{\rm sym}$ are listed, while η, ξ, η_{sy}, and ξ_{sy} are specific combinations with them given by $\eta = (K_0 L^2)^{1/3}$, $\xi = |Q^6 K_{\rm sym}/Q_{\rm sym}|^{1/6}$, $\eta_{sy} = [(K_0 + K_{\rm sym})L^2]^{1/3}$, and $\xi_{sy} = |Q^{11} K_{\rm sym}/Q_{\rm sym}|^{1/11}$. In addition, we also list the TOV mass of the neutron stars constructed with the EOSs listed here with the central density $n_c = 3n_0$.

EOS	K_0 (MeV)	n_0 (fm^{-3})	L (MeV)	Q (MeV)	$K_{\rm sym}$ (MeV)	$Q_{\rm sym}$ (MeV)	η (MeV)	ξ (MeV)	η_{sy} (MeV)	ξ_{sy} (MeV)	$M_{n_c/n_0=3}$ ($M_\odot$)
OI-EOSs	200	0.165	35.6	−759	−142	801	63.3	569	41.8	649	0.68
		0.165	67.8	−761	−27.6	589	97.2	457	92.5	576	1.17
	220	0.161	40.2	−720	−144	731	70.9	549	49.7	621	0.81
		0.161	77.6	−722	−9.83	486	110	377	108	506	1.32
	240	0.159	45.0	−663	−146	642	78.6	518	57.6	579	0.95
		0.158	88.2	−664	10.5	363	123	368	125	482	1.47
	260	0.156	49.8	−589	−146	535	86.4	474	65.6	523	1.09
		0.155	99.2	−590	32.6	219	137	429	142	496	1.61
	280	0.154	54.9	−496	−146	410	94.5	418	73.8	452	1.23
		0.153	111	−498	57.4	54.4	151	502	161	500	1.76
	300	0.152	60.0	−386	−146	266	103	349	82.2	366	1.38
		0.151	124	−387	86.1	−133	167	360	181	372	1.90
KDE0v	229	0.161	45.2	−373	−145	523	77.6	301	55.6	332	1.11
KDE0v1	228	0.165	54.7	−385	−127	484	88.0	308	67.0	341	1.19
SLy2	230	0.161	47.5	−364	−115	507	80.3	285	63.7	318	1.26
SLy4	230	0.160	45.9	−363	−120	522	78.7	284	61.6	318	1.22
SLy9	230	0.151	54.9	−350	−81.4	462	88.4	262	76.4	299	1.41
SKa	263	0.155	74.6	−300	−78.5	175	114	263	101	279	1.57
SkI3	258	0.158	101	−304	73.0	212	138	254	150	276	1.77
SkMp	231	0.157	70.3	−338	−49.8	159	105	278	96.4	304	1.45
Shen	281	0.145	111	…	33.5	…	151	…	157	…	1.82
Togashi	245	0.160	38.7	…	…	…	71.6	…	…	…	1.27

The coefficients in these expressions are the nuclear saturation parameters, with which each EOS is characterized. The parameters for the adopted EOSs are concretely listed in Table I, where η, ξ, η_{sy}, and ξ_{sy} are the specific combination of the nuclear saturation parameters (see the following sections for details), defined by

$$\eta = (K_0 L^2)^{1/3}, \tag{4}$$

$$\xi = \left| \frac{Q^6 K_{\rm sym}}{Q_{\rm sym}} \right|^{1/6}, \tag{5}$$

$$\eta_{sy} = [(K_0 + K_{\rm sym})L^2]^{1/3}, \tag{6}$$

$$\xi_{sy} = \left| \frac{Q^{11} K_{\rm sym}}{Q_{\rm sym}} \right|^{1/11}. \tag{7}$$

Among the nuclear saturation parameters, n_0, w_0, and S_0 are well constrained as $n_0 \approx 0.15$–0.16 fm^{-3}, $w_0 \approx -15.8$ MeV [39], and $S_0 \approx 31.6 \pm 2.7$ MeV [40]. Meanwhile, K_0 and L are more difficult to be determined from the terrestrial experiments, because these parameters are the density derivative at the saturation point; i.e., one needs to know the information not only at the saturation point but also in a wider range around the saturation point. The constraints on these parameters are gradually improved and the current fiducial values are $K_0 = 230 \pm 40$ [41] and $L = 58.9 \pm 16$ MeV [40], even though the constraints on L recently reported from two large facilities still have a large uncertainty, i.e., $42 \le L \le 117$ MeV with SπRIT by the Radioactive Isotope Beam Factory at RIKEN in Japan [26] and $L = 106 \pm 37$ MeV with PREX-II by the Thomas Jefferson National Accelerator Facility in Newport News, Virginia, U.S. [27]. Moreover, the saturation parameters in higher order terms, such as Q, $K_{\rm sym}$, and $Q_{\rm sym}$, are almost unconstrained from the experiments, but they are theoretically predicted as $-800 \le Q \le 400$, $-400 \le K_{\rm sym} \le 100$, and $-200 \le Q_{\rm sym} \le 800$ MeV [40].

It is known that S_0 is strongly associated with L as $S_0 \approx 28 + 0.075L$ [29,42]. In a similar way, we find that $K_0 + K_{\rm sym}$ is also strongly associated with L, adopting 118 models for the Skyrme-type EOSs listed in Ref. [43] and 304 models for OI-EOSs. We plot $K_0 + K_{\rm sym}$ as a function of L in Fig. 2, where the thick solid line denotes the fitting formula given by

$$K_0 + K_{\rm sym} = -75.86 + 371.8\left(\frac{L}{100\ \text{MeV}}\right). \tag{8}$$

The similar correlation has been reported in Ref. [44], which is shown in Fig. 2 with the dotted line. This type of correlation may be very useful for constraining the value of $K_{\rm sym}$ with using the constraints on K_0 and L, because the uncertainty in $K_{\rm sym}$ is still very large. In practice, by

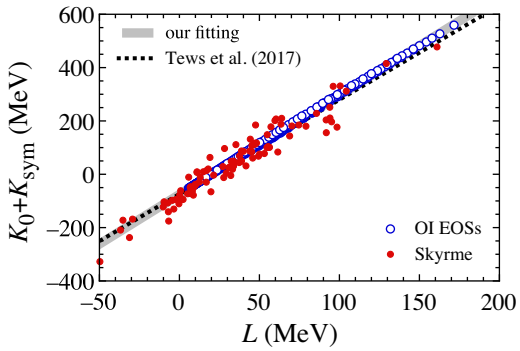

FIG. 2. The relation between $K_0 + K_{sym}$ and L for the OI-EOSs and Skyrme-type EOSs. The solid line denotes the fitting given by Eq. (8), while the dotted line denotes the fitting proposed in the previous study [44].

assigning the fiducial values of K_0 and L mentioned above in Eq. (8), one can find that $-186 \leq K_{sym} \leq 13$ MeV.

III. NEUTRON STAR MASS FORMULA

The neutron star structure is determined by solving the TOV equations together with the appropriate EOS. The neutron star may sometimes be considered as a huge nucleus, but its structure is quite dense, compered to atomic nuclei. Nevertheless, since the density inside low-mass neutron stars is definitely low, their mass seems to be strongly associated with the nuclear saturation properties. In practice, it has been found that the mass M and gravitational redshift $z \equiv (1-2GM/Rc^2)^{-1/2} - 1$, for the low-mass neutron stars, whose central density is less than twice the nuclear saturation density, are well expressed as a function of η defined by Eq. (4) and $u_c = \rho_c/\rho_0$, where ρ_c and ρ_0 are the central energy density and the energy density corresponding to the nuclear saturation density, i.e., $\rho_0 = 2.68 \times 10^{14}$ g/cm^3 [28]. That is, one can estimate neutron star mass and radius by combining the empirical formulas $M = M(u_c, \eta)$ and $z = z(u_c, \eta)$. In practice, assuming the recent experimental constraints obtained with SπRIT and PREX-II [26,27], one can show the allowed region in the neutron star mass and radius relation [45]. Using this new parameter η, one can also discuss the rotational properties of the low-mass neutron stars [46] and the possible maximum mass of neutron stars [47,48]. In this study, we try to extend this type of empirical formulas even for higher central density up to 3 times saturation density. This is because, as the central density becomes larger, the empirical formulas discussed in more detail below lose accuracy. This may come from the additional EOS dependence, such as higher order coefficients in Eqs. (2) and (3). In addition, for reference, we show the mass of neutron stars with $n_c = 3n_0$ constructed with the EOSs considered in this study in Table I, with which one may be able to adopt our empirical relations discussed below if the stellar mass is less than $\simeq 0.68$–$1.90 M/M_\odot$ (average value is $1.34\,M_\odot$).

A. Function of η

Since the saturation density n_0 also depends on the EOS models, as shown in Table I, it may be better to consider the mass and redshift for the low-mass neutron star as a function of n_c/n_0 instead of ρ_c/ρ_0 with the fixed value of ρ_0, where n_c is the baryon number density at the stellar center. In fact, as shown in Fig. 3, one can observe that the neutron star mass M and gravitational redshift z with the fixed central baryon number density, e.g., $n_c/n_0 = 1$, 2, 3, are strongly correlated with η. We note that M and z have a quite similar dependence on η, even though each value is completely different, as shown in Ref. [28]. With this result, we can derive the fitting formulas as

$$\frac{M_\eta}{M_\odot} = a_0^m + a_1^m \ln(\eta_{100}) + a_2^m \eta_{100} + a_3^m \eta_{100}^2, \quad (9)$$

$$z_\eta = a_0^z + a_1^z \ln(\eta_{100}) + a_2^z \eta_{100} + a_3^z \eta_{100}^2, \quad (10)$$

where $\eta_{100} \equiv \eta/(100\ \text{MeV})$, while a_i^m and a_i^z for $i = 0$–3 are the coefficients in the fitting formulas, depending on the normalized central density, $\mathcal{R}_c \equiv n_c/n_0$. Here, in order to distinguish the mass and radius determined by integrating TOV equations with each EOS, the mass and redshift estimated with the fitting formulas given by Eqs. (9) and (10) are referred to as M_η and z_η. In addition, as shown in Fig. 4, we find that the coefficients a_i^m and a_i^z are well expressed as a function of $\mathcal{R}_c$ as

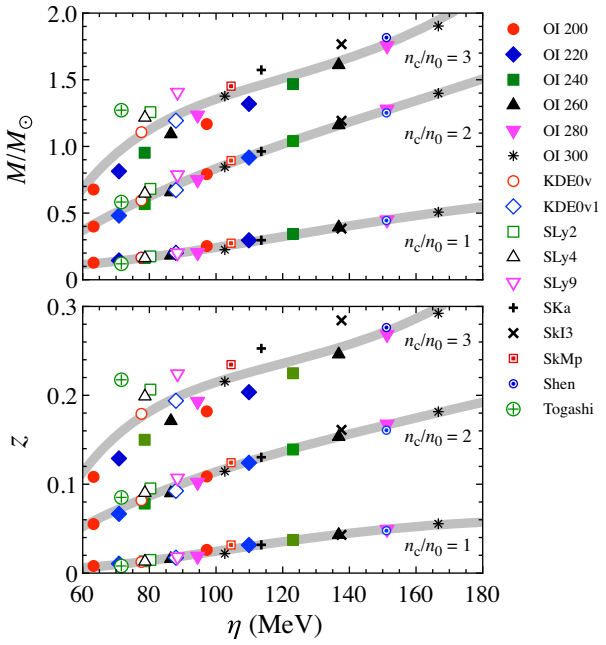

FIG. 3. The neutron star mass M and gravitational redshift z for various EOSs with the fixed central baryon number density, $n_c/n_0 = 1$, 2, 3, are plotted as a function of η. The thick, solid lines denote the fitting lines given by Eqs. (9) and (10).

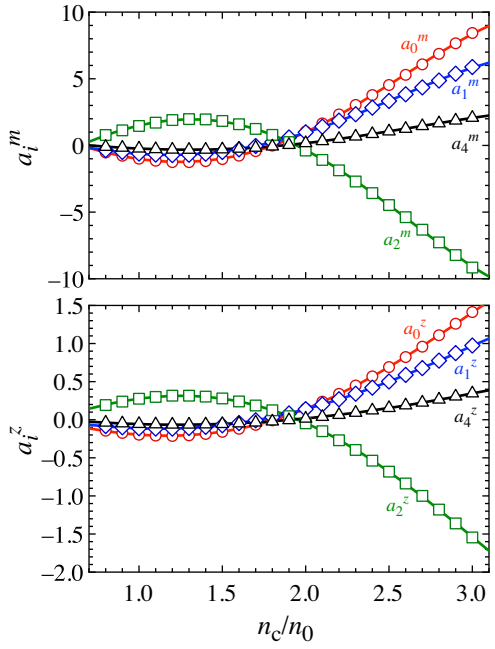

FIG. 4. The n_c/n_0 dependence of the coefficients a_i^m and a_i^z in the fitting formula of stellar mass and gravitational redshift as a function of $\eta/(100\ \mathrm{MeV})$ expressed by Eqs. (9) and (10). The open marks denote the values of a_i^m and a_i^z in the fitting formulas, while the solid lines denote the fitting as a function of n_c/n_0 as in Eqs. (11) and (12).

$$a_i^m(\mathcal{R}_c) = a_{i0}^m + a_{i1}^m \mathcal{R}_c + a_{i2}^m \mathcal{R}_c^3 + a_{i3}^m \mathcal{R}_c^5, \quad (11)$$

$$a_i^z(\mathcal{R}_c) = a_{i0}^z + a_{i1}^z \mathcal{R}_c + a_{i2}^z \mathcal{R}_c^3 + a_{i3}^z \mathcal{R}_c^5, \quad (12)$$

where the exact values of a_{ij}^m and a_{ij}^z for $i = 0$–3 and $j = 0$–3 are listed in Table II. Now, we can get the empirical formulas for the neutron star mass and redshift as $M_\eta = M_\eta(\mathcal{R}_c, \eta)$ and $z_\eta = z_\eta(\mathcal{R}_c, \eta)$ given by Eqs. (9)–(12).

Next, in order to improve the resultant empirical formulas, we try to characterize the deviation of the neutron star mass and redshift determined with each EOS from those estimated with the fitting formulas given by Eqs. (9)–(12), using a specific combination of the nuclear saturation parameters in the higher order terms. That is, the deviation of the mass and redshift are given by

$$\Delta M_\eta = M_{\mathrm{TOV}} - M_\eta(\mathcal{R}_c, \eta), \quad (13)$$

$$\Delta z_\eta = z_{\mathrm{TOV}} - z_\eta(\mathcal{R}_c, \eta), \quad (14)$$

where M_{TOV} and z_{TOV} are the neutron star mass and redshift determined by integrating the TOV equations together with each EOS. Through a trial and error process, we find a good combination of K_{sym}, Q, and Q_{sym}, which is ξ defined by Eq. (5), for characterizing ΔM_η and Δz_η, even though it may be a not so tight correlation. We note that it may be necessary to modify the definition of ξ, if ξ is out of the range considered in this study, i.e., $250 \lesssim \xi \lesssim 600$ MeV with the EOSs adopted in this study. In fact, ξ is not defined when $Q_{\mathrm{sym}} = 0$. In practice, for the neutron star models with $n_c/n_0 = 2$ and 3, we show $\Delta M_\eta/M_\odot$ and z_η as a function of ξ in Fig. 5, considering the OI-EOSs and the Skyrme-type EOSs. In this figure, we also plot the fitting formulas given by

$$\frac{\Delta M_\eta}{M_\odot} = b_0^m/\xi_{500} + b_1^m \xi_{500} + b_2^m \xi_{500}^2 + b_3^m \xi_{500}^3, \quad (15)$$

$$\Delta z_\eta = b_0^z/\xi_{500} + b_1^z \xi_{500} + b_2^z \xi_{500}^2 + b_3^z \xi_{500}^3, \quad (16)$$

TABLE II. Values of a_{ij}^m and a_{ij}^z in Eqs. (11) and (12).

j	0	1	2	3
a_{0j}^m	3.2110	−5.5024	1.3375	−0.059490
a_{1j}^m	1.8340	−3.2893	0.87206	−0.039859
a_{2j}^m	−4.3905	7.4582	−1.6450	0.071406
a_{3j}^m	0.94544	−1.5004	0.33522	− 0.014110
a_{0j}^z	0.25385	−0.60188	0.15808	−0.0053861
a_{1j}^z	0.15141	−0.36133	0.10275	−0.0035881
a_{2j}^z	−0.38040	0.84306	−0.19442	0.0064246
a_{3j}^z	0.086653	−0.18150	0.041746	−0.0013309

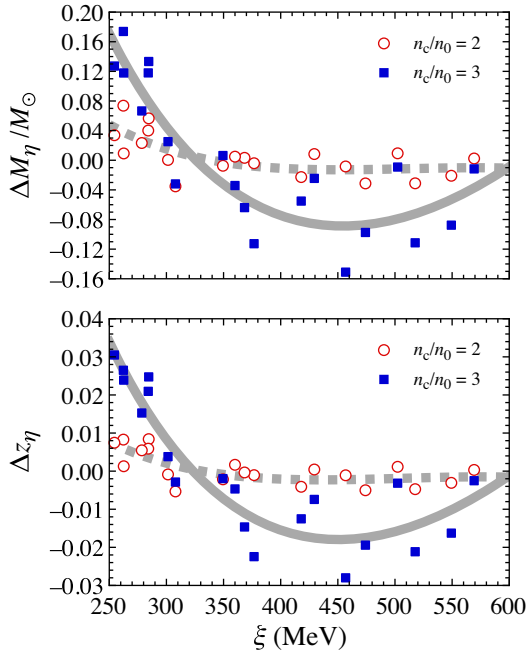

FIG. 5. Considering the OI-EOSs and the Skyrme-type EOSs, $\Delta M_\eta/M_\odot$ and z_η calculated with Eqs. (13) and (14) are shown as a function of ξ for $n_c/n_0 = 2$ (open circles) and 3 (filled squares). The dotted and solid lines are fitting lines given by Eqs. (15) and (16).

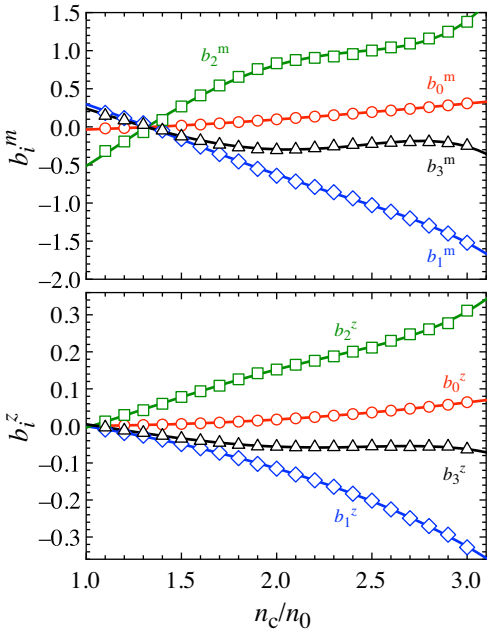

FIG. 6. The coefficients in Eqs. (15) and (16) are shown as a function of n_c/n_0 with marks, while the solid lines denote the fitting given by Eqs. (17) and (18), respectively.

where $\xi_{500} \equiv \xi/(500\ \mathrm{MeV})$, while again b_i^m and b_i^z for $i = 0$–3 are the adjusting coefficients depending on $\mathcal{R}_c$. In a similar way for deriving the fitting formulas for ΔM_η and Δz_η, the coefficients in Eqs. (15) and (16) are plotted in Fig. 6 as a function of n_c/n_0, which can be fitted with

$$b_i^m(\mathcal{R}_c) = b_{i0}^m + b_{i1}^m \mathcal{R}_c^2 + b_{i2}^m \mathcal{R}_c^4 + b_{i3}^m \mathcal{R}_c^6, \quad (17)$$

$$b_i^z(\mathcal{R}_c) = b_{i0}^z + b_{i1}^z \mathcal{R}_c^2 + b_{i2}^z \mathcal{R}_c^4 + b_{i3}^z \mathcal{R}_c^6, \quad (18)$$

where the concrete values of the coefficients b_{ij}^m and b_{ij}^z for $i = 0$–3 and $j = 0$–3 are listed in Table III. We note that we consider the fitting of ΔM_η and Δz_η only for $n_c/n_0 > 1$ as in Fig. 6, even though, in principle, one can also fit them for a lower density region. This is because the correlation of ΔM_η and Δz_η with ξ becomes weaker and the absolute values of ΔM_η and Δz_η become much smaller, as the density becomes lower. So, for $n_c/n_0 \le 1$ we simply assume that $\Delta M_\eta = 0$ and $\Delta z_\eta = 0$ in this study.

Now, we can derive new empirical formulas for the neutron star mass $M_{\eta\xi}$ and redshift $z_{\eta\xi}$ as a function of $\mathcal{R}_c (= n_c/n_0)$, η, and ξ,

$$\frac{M_{\eta\xi}}{M_\odot} = \frac{M_\eta(\mathcal{R}_c,\eta)}{M_\odot} + \frac{\Delta M_\eta(\mathcal{R}_c,\xi)}{M_\odot}, \quad (19)$$

$$z_{\eta\xi} = z_\eta(\mathcal{R}_c,\eta) + \Delta z_\eta(\mathcal{R}_c,\xi), \quad (20)$$

where the first terms are given by Eqs. (9)–(12) and the second terms are given by Eqs. (15)–(18). In order to check the accuracy of our empirical formulas, $M_\eta(\mathcal{R}_c,\eta)$, $z_\eta(\mathcal{R}_c,\eta)$, $M_{\eta\xi}(\mathcal{R}_c,\eta,\xi)$, and $z_{\eta\xi}(\mathcal{R}_c,\eta,\xi)$, in Fig. 7 we show the relative deviation from the neutron star mass and redshift determined through the TOV equations, where the bottom panels are the relative deviation of the neutron star radius estimated with the empirical formulas for the mass and redshift from the TOV solution. From this figure, one can see that the neutron star mass is estimated within ∼10% accuracy, while the radius for the canonical neutron star is estimated within ∼3% accuracy, using the empirical formulas $M_{\eta\xi}(\mathcal{R}_c,\eta,\xi)$ and $z_{\eta\xi}(\mathcal{R}_c,\eta,\xi)$. We also make a comment that the mass estimation with $M_\eta(\mathcal{R}_c,\eta)$ (top left panel) is better than that with $M_{\eta\xi}(\mathcal{R}_c,\eta,\xi)$ (top right panel) in the density region around $n_c/n_0 \simeq 1.5$, which comes from the fact that the correlation between ΔM_η and ξ becomes worse as the density becomes lower. We note that the mass and gravitational redshift have quite similar dependence on η, as shown in Fig. 3; i.e., it seems to get a small amount of difference in information from the mass and gravitational redshift. Even so, one can accurately recover the radius, using the empirical relations for the mass and gravitational redshift.

At the end, we mention another possibility for characterizing ΔM_η and Δz_η instead of ξ. In practice, we find that a new parameter $\xi_{\mathcal{R}_c}$, defined by

TABLE III. Values of b_{ij}^m and b_{ij}^z in Eqs. (17) and (18).

j	0	1	2	3
b_{0j}^m	-7.711×10^{-2}	4.122×10^{-2}	8.051×10^{-4}	-7.267×10^{-5}
b_{1j}^m	7.763×10^{-1}	-5.341×10^{-1}	5.793×10^{-2}	-2.995×10^{-3}
b_{2j}^m	-1.470	1.123	-1.774×10^{-1}	9.771×10^{-3}
b_{3j}^m	7.276×10^{-1}	-5.897×10^{-1}	1.077×10^{-1}	-6.041×10^{-3}
b_{0j}^z	-2.783×10^{-3}	1.679×10^{-3}	9.658×10^{-4}	-3.707×10^{-5}
b_{1j}^z	3.989×10^{-2}	-4.167×10^{-2}	1.204×10^{-3}	-1.209×10^{-4}
b_{2j}^z	-9.514×10^{-2}	1.031×10^{-1}	-1.341×10^{-2}	7.713×10^{-4}
b_{3j}^z	5.321×10^{-2}	-5.814×10^{-2}	9.859×10^{-3}	-5.368×10^{-4}

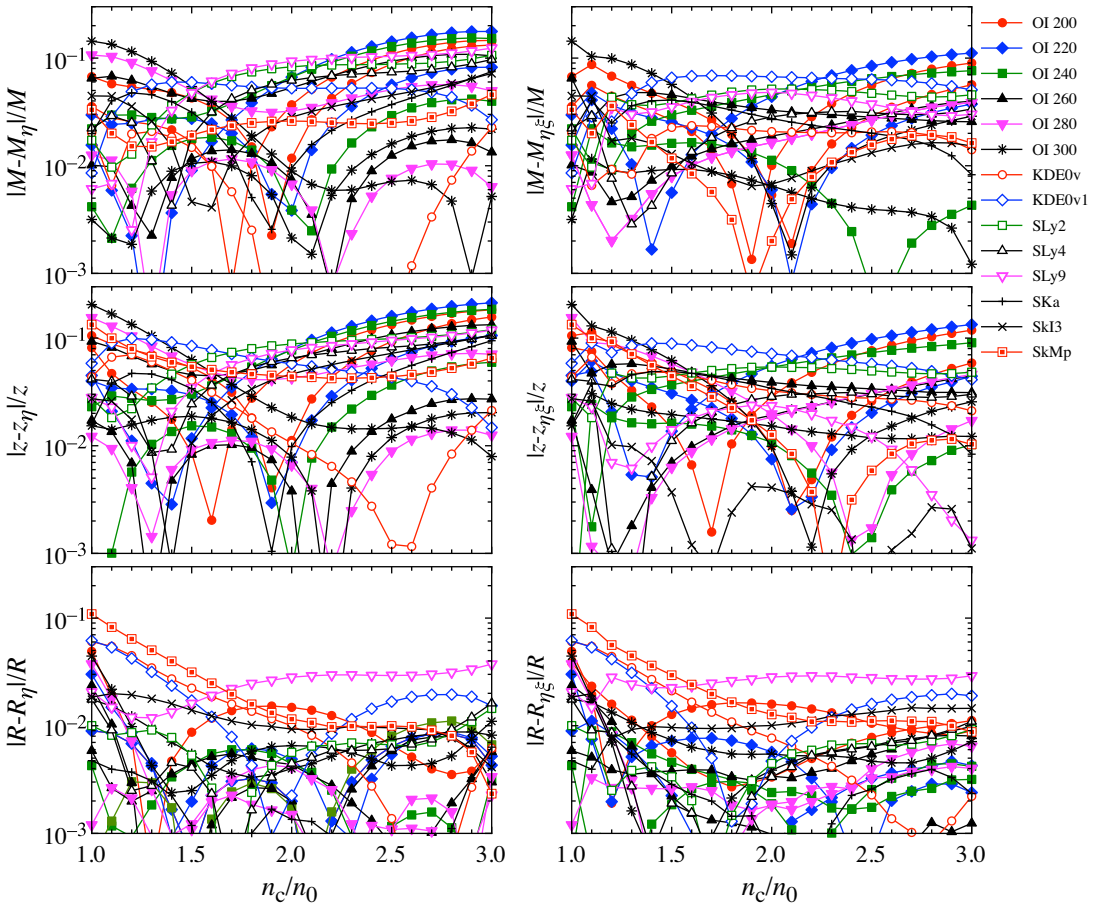

FIG. 7. Relative deviation of the neutron star mass (top) and redshift (middle) estimated with the empirical formulas from those constructed with each EOS are shown as a function of the normalized central baryon number density. Left: the deviation with the empirical formulas $M_\eta(\mathcal{R}_c,\eta)$ and $z_\eta(\mathcal{R}_c,\eta)$. Right: deviation with $M_{\eta\xi}(\mathcal{R}_c,\eta,\xi)$ and $z_{\eta\xi}(\mathcal{R}_c,\eta,\xi)$. Bottom: the relative deviation of the neutron star radius estimated with the empirical formulas for the mass and redshift from that calculated with each EOS.

$$\xi_{\mathcal{R}_c} = \left|\frac{Q^{2\mathcal{R}_c}K_{\rm sym}}{Q_{\rm sym}}\right|^{1/2\mathcal{R}_c}, \tag{21}$$

seems to be better than ξ given by Eq. (5) for characterizing ΔM_η and Δz_η. That is, adopting the same functional form as Eqs. (15) and (16), one can express ΔM_η and Δz_η with $\xi_{\mathcal{R}_c}$, where the correlation in a lower density region is better than the case with ξ. But, unfortunately, the dependence of the coefficients b_i^m and b_i^z on $\mathcal{R}_c$ becomes more complex. So, in this study, we simply adopt ξ as mentioned above.

B. Function of η_{sy}

Up to now we consider to derive the empirical formulas with η, but another combination of the nuclear saturation parameters may be better to express the neutron star mass and redshift. Here, we consider to derive the empirical formulas as a function of η_{sy} defined by Eq. (8) instead of η. In Fig. 8, we plot the neutron star mass and redshift with $n_c/n_0 = 1$, 2, 3 constructed with each EOS, together with the fitting lines given by

$$\frac{M_{\eta_{sy}}}{M_\odot} = a^m_{sy,0} + a^m_{sy,1}\ln(\eta_{sy,100}) + a^m_{sy,2}\eta_{sy,100} + a^m_{sy,3}\eta^2_{sy,100}, \tag{22}$$

$$z_{\eta_{sy}} = a^z_{sy,0} + a^z_{sy,1}\ln(\eta_{sy,100}) + a^z_{sy,2}\eta_{sy,100} + a^z_{sy,3}\eta^2_{sy,100}, \tag{23}$$

where $\eta_{sy,100} \equiv \eta_{sy}/(100\ \text{MeV})$. Again, the coefficients $a^m_{sy,i}$ and $a^z_{sy,i}$ depend on $\mathcal{R}_c$, which are shown in Fig. 9. In this figure, the marks denote numerical values determined by fitting with Eqs. (22) and (23) as in Fig. 8, while the solid lines denote the fitting of $a^m_{sy,i}$ and $a^z_{sy,i}$ as a function of $\mathcal{R}_c$ with

$$a^m_{sy,i}(\mathcal{R}_c) = a^m_{sy,i0} + a^m_{sy,i1}\mathcal{R}_c + a^m_{sy,i2}\mathcal{R}_c^3 + a^m_{sy,i3}\mathcal{R}_c^5, \tag{24}$$

$$a^z_{sy,i}(\mathcal{R}_c) = a^z_{sy,i0} + a^z_{sy,i1}\mathcal{R}_c + a^z_{sy,i2}\mathcal{R}_c^3 + a^z_{sy,i3}\mathcal{R}_c^5, \tag{25}$$

where the concrete values of $a^m_{sy,ij}$ and $a^z_{sy,ij}$ for $i = 0$–3 and $j = 0$–3 are listed in Table IV. Comparing Fig. 8 to Fig. 3,

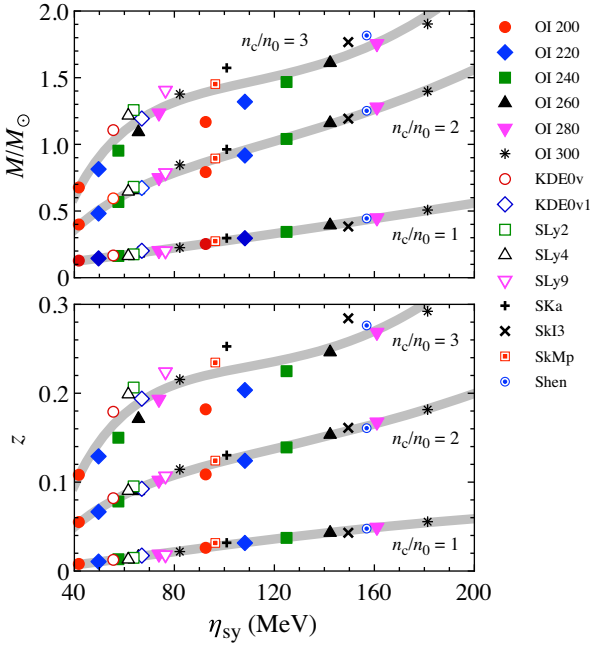

FIG. 8. Same as in Fig. 3, but as a function of η_{sy}. The thick, solid lines denote the fitting lines given by Eqs. (22) and (23).

η seems to be better than η_{sy} in this stage, because a specific EOS model (e.g., OI 220) with $n_c/n_0 = 3$ largely deviates from the fitting line in Fig. 8.

Then, we consider to characterize the deviation of the neutron star mass and redshift estimated with the empirical formulas $M_{\eta_{sy}}(\mathcal{R}_c, \eta_{sy})$ and $z_{\eta_{sy}}(\mathcal{R}_c, \eta_{sy})$, given

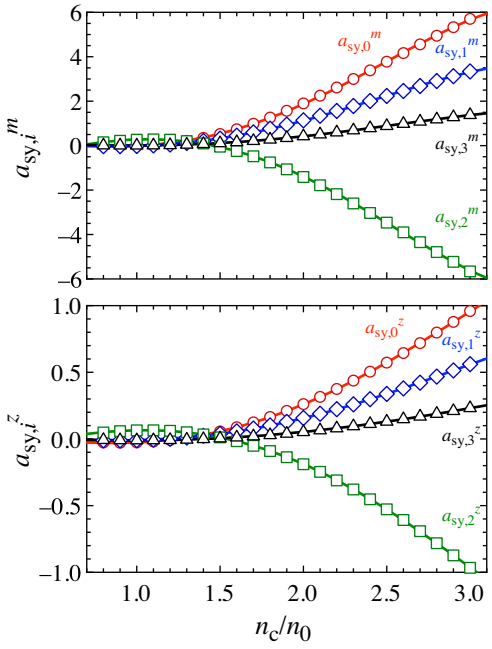

FIG. 9. The coefficients in Eqs. (22) and (23) are plotted as a function of $\mathcal{R}_c = n_c/n_0$, while the solid lines are the corresponding fitting given by Eqs. (24) and (23).

TABLE IV. Values of $a_{sy,ij}^m$ and $a_{sy,ij}^z$ in Eqs. (24) and (25).

j	0	1	2	3
$a_{sy,0j}^m$	0.6990	−1.2408	0.5655	−0.02710
$a_{sy,1j}^m$	0.3220	−0.6504	0.3266	−0.01596
$a_{sy,2j}^m$	−1.2165	2.1443	−0.6833	0.03134
$a_{sy,3j}^m$	0.2314	−0.3555	0.1374	−0.006172
$a_{sy,0j}^z$	0.05286	−0.1492	0.07355	−0.002614
$a_{sy,1j}^z$	0.03503	−0.08519	0.04252	−0.001517
$a_{sy,2j}^z$	−0.1233	0.2726	−0.08809	0.002965
$a_{sy,3j}^z$	0.02629	−0.05430	0.01929	−0.0006297

by Eqs. (22)–(25) from those determined as the TOV solution. Such a deviation is given by

$$\Delta M_{\eta_{sy}} = M_{\rm TOV} - M_{\eta_{sy}}(\mathcal{R}_c, \eta_{sy}), \tag{26}$$

$$\Delta z_{\eta_{sy}} = z_{\rm TOV} - z_{\eta_{sy}}(\mathcal{R}_c, \eta_{sy}). \tag{27}$$

In the beginning, we try to characterize $\Delta M_{\eta_{sy}}$ and $\Delta z_{\eta_{sy}}$ with a specific combination of Q and $Q_{\rm sym}$, because $K_{\rm sym}$ is already included in the definition of η_{sy}, but eventually we find that the combination of $K_{\rm sym}$, Q, and $Q_{\rm sym}$ defined by Eq. (7) are suitable for this problem. In fact, as shown in Fig. 10, $\Delta M_{\eta_{sy}}$ and $\Delta z_{\eta_{sy}}$ are well fitted as a function of ξ_{sy}, where the open circles (filled squares) denote the values of $\Delta M_{\eta_{sy}}$ and $\Delta z_{\eta_{sy}}$ with $n_c/n_0 = 2$ ($n_c/n_0 = 3$), while the

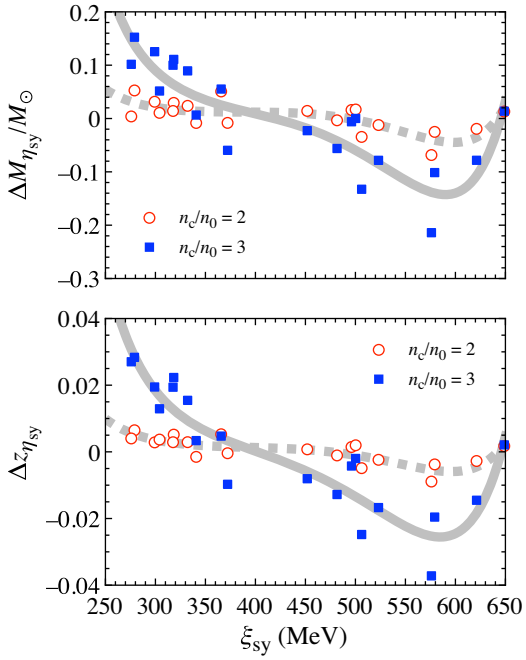

FIG. 10. $\Delta M_{\eta_{sy}}$ and $\Delta z_{\eta_{sy}}$ with $n_c/n_0 = 2$ and 3 are plotted as a function of ξ_{sy}, where the thick, solid lines for $n_c/n_0 = 3$ and thick, dotted lines for $n_c/n_0 = 2$ are fitting lines given by Eqs. (28) and (29).

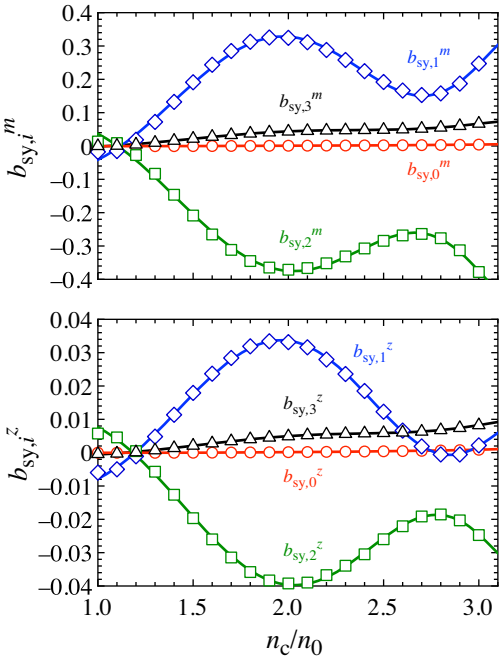

FIG. 11. The coefficients in the fitting formulas [Eqs. (28) and (29)] $b_{sy,i}^m$ and $b_{sy,i}^z$ for $i = 0$–3 are plotted as a function of n_c/n_0, while the solid lines are the fitting of those values as n_c/n_0 with the functional form given by Eqs. (30)–(29).

dotted (solid) lines denote the fitting of those values with $n_c/n_0 = 2$ ($n_c/n_0 = 3$) by

$$\frac{\Delta M_{\eta_{sy}}}{M_\odot} = b_{sy,0}^m/\xi_{sy,500}^6 + b_{sy,1}^m\xi_{sy,500}^7 + b_{sy,2}^m\xi_{sy,500}^8 + b_{sy,3}^m\xi_{sy,500}^{12}, \tag{28}$$

$$\Delta z_{\eta_{sy}} = b_{sy,0}^z/\xi_{sy,500}^6 + b_{sy,1}^z\xi_{sy,500}^7 + b_{sy,2}^z\xi_{sy,500}^8 + b_{sy,3}^z\xi_{sy,500}^{12}. \tag{29}$$

In these fitting formulas, $\xi_{sy,500}$ is defined as $\xi_{sy,500} \equiv \xi_{sy}/(500\ \mathrm{MeV})$, while $b_{sy,i}^m$ and $b_{sy,i}^z$ for $i = 0$–3 are the adjusting coefficients, depending on n_c/n_0. In Fig. 11, the values of $b_{sy,i}^m$ and $b_{sy,i}^z$ for $i = 0$–3 are plotted as a function of n_c/n_0, where the solid lines are the fitting of those values with the functional form given by

$$b_{sy,0}^m(\mathcal{R}_c) = b_{sy,00}^m\mathcal{R}_c^2 + b_{sy,01}^m\mathcal{R}_c^4 + b_{sy,02}^m\mathcal{R}_c^6 + b_{sy,03}^m\mathcal{R}_c^9, \tag{30}$$

$$b_{sy,i}^m(\mathcal{R}_c) = b_{sy,i0}^m\mathcal{R}_c^2 + b_{sy,i1}^m\mathcal{R}_c^4 + b_{sy,i2}^m\mathcal{R}_c^5 + b_{sy,i3}^m\mathcal{R}_c^7 + b_{sy,i4}^m\mathcal{R}_c^9, \tag{31}$$

$$b_{sy,0}^z(\mathcal{R}_c) = b_{sy,00}^z\mathcal{R}_c^3 + b_{sy,01}^z\mathcal{R}_c^4 + b_{sy,02}^z\mathcal{R}_c^8 + b_{sy,03}^z\mathcal{R}_c^9, \tag{32}$$

$$b_{sy,i}^z(\mathcal{R}_c) = b_{sy,i0}^z\mathcal{R}_c^2 + b_{sy,i1}^z\mathcal{R}_c^4 + b_{sy,i2}^z\mathcal{R}_c^5 + b_{sy,i3}^z\mathcal{R}_c^7 + b_{sy,i4}^z\mathcal{R}_c^9. \tag{33}$$

The coefficients in these equations, $b_{sy,ij}^m$ and $b_{sy,ij}^z$, are concretely listed in Table V.

Now, we get the alternative empirical formulas for the neutron star mass and gravitational redshift as a function of $\mathcal{R}_c$, η_{sy}, and ξ_{sy},

$$\frac{M_{\eta\xi_{sy}}}{M_\odot} = \frac{M_{\eta_{sy}}(\mathcal{R}_c,\eta_{sy})}{M_\odot} + \frac{\Delta M_{\eta_{sy}}(\mathcal{R}_c,\xi_{sy})}{M_\odot}, \tag{34}$$

$$z_{\eta\xi_{sy}} = z_{\eta_{sy}}(\mathcal{R}_c,\eta_{sy}) + \Delta z_{\eta_{sy}}(\mathcal{R}_c,\xi_{sy}), \tag{35}$$

where the first terms are given by Eqs. (22)–(25) and the second terms are given by Eqs. (28)–(33). In order to check how well one can estimate the neutron star mass and gravitational redshift with the empirical formulas with η_{sy}, i.e., $M_{\eta_{sy}}(\mathcal{R}_c,\eta_{sy})$, $z_{\eta_{sy}}(\mathcal{R}_c,\eta_{sy})$, $M_{\eta\xi_{sy}}(\mathcal{R}_c,\eta_{sy},\xi_{sy})$, and $z_{\eta\xi_{sy}}(\mathcal{R}_c,\eta_{sy},\xi_{sy})$, we calculate the relative deviation from the TOV solutions constructed with concrete EOSs and show the absolute value of it in Fig. 12, where the top and middle panels correspond to the mass and gravitational

TABLE V. Values of $b_{sy,ij}^m$ and $b_{sy,ij}^z$ in Eqs. (30)–(33).

j	0	1	2	3	4
$b_{sy,0j}^m$	-9.146×10^{-4}	4.823×10^{-4}	-5.734×10^{-5}	7.712×10^{-7}	…
$b_{sy,1j}^m$	-3.719×10^{-1}	6.652×10^{-1}	-3.572×10^{-1}	2.324×10^{-2}	-7.279×10^{-4}
$b_{sy,2j}^m$	3.684×10^{-1}	-6.647×10^{-1}	3.551×10^{-1}	-2.302×10^{-2}	7.217×10^{-4}
$b_{sy,3j}^m$	-2.956×10^{-2}	5.484×10^{-2}	-2.879×10^{-2}	1.839×10^{-3}	-5.768×10^{-5}
$b_{sy,0j}^z$	-1.032×10^{-4}	7.160×10^{-5}	-1.388×10^{-6}	3.541×10^{-7}	…
$b_{sy,1j}^z$	-4.730×10^{-2}	7.798×10^{-2}	-4.105×10^{-2}	2.563×10^{-3}	-7.723×10^{-5}
$b_{sy,2j}^z$	4.726×10^{-2}	-7.785×10^{-2}	4.065×10^{-2}	-2.522×10^{-3}	7.586×10^{-5}
$b_{sy,3j}^z$	-3.880×10^{-3}	6.386×10^{-3}	-3.246×10^{-3}	1.967×10^{-4}	-5.867×10^{-6}

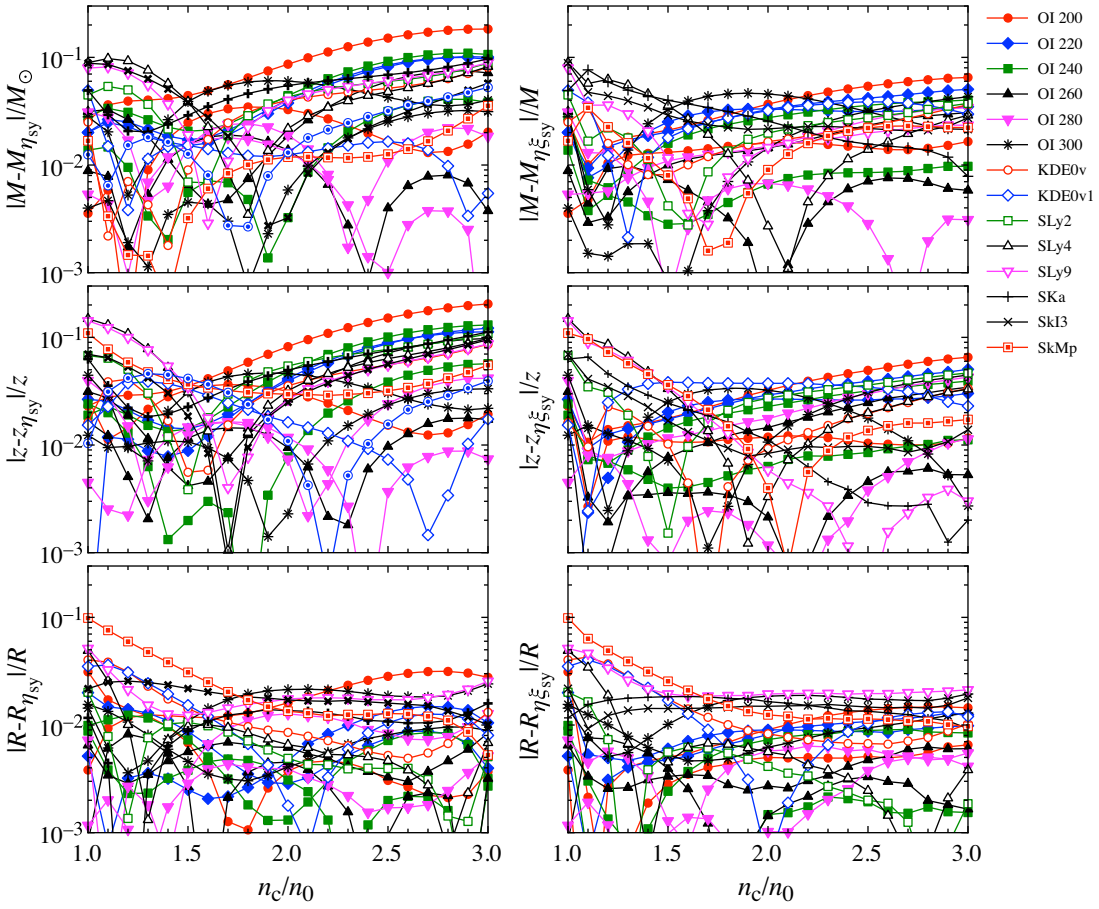

FIG. 12. Same as Fig. 7, but with the empirical formulas $M_{\eta_{sy}}(\mathcal{R}_c, \eta_{sy})$, $z_{\eta_{sy}}(\mathcal{R}_c, \eta_{sy})$, $M_{\eta\xi_{sy}}(\mathcal{R}_c, \eta_{sy}, \xi_{sy})$, and $z_{\eta\xi_{sy}}(\mathcal{R}_c, \eta_{sy}, \xi_{sy})$.

redshift, while the bottom panels are the relative deviation of the radius estimated with the empirical formulas for mass and gravitational redshift. Comparing to Fig. 7, one can see that the empirical formulas with η_{sy} are the same level as or better than those with η. In fact, with respect to the canonical neutron star models, one can estimate the mass (radius) within ∼7% (∼2%) accuracy, using the empirical relations $M_{\eta\xi_{sy}}(\mathcal{R}_c, \eta_{sy}, \xi_{sy})$ and $z_{\eta\xi_{sy}}(\mathcal{R}_c, \eta_{sy}, \xi_{sy})$. We note that one can accurately estimate the radius by using the empirical formulas for the mass and gravitational redshift again, even though the dependence of the mass and gravitational redshift on η_{sy} are quite similar, as show in Fig. 8.

TABLE VI. Correspondence between the empirical formulas and their equations.

Empirical formula	Corresponding equations
$M_\eta(\mathcal{R}_c, \eta)$	(9) and (11)
$M_{\eta\xi}(\mathcal{R}_c, \eta, \xi)$	(19) with (9), (11), (15), and (17)
$M_{\eta_{sy}}(\mathcal{R}_c, \eta_{sy})$	(22) and (24)
$M_{\eta\xi_{sy}}(\mathcal{R}_c, \eta_{sy}, \xi_{sy})$	(34) with (22), (24), (28), (30), and (31)
$z_\eta(\mathcal{R}_c, \eta)$	(10) and (12)
$z_{\eta\xi}(\mathcal{R}_c, \eta, \xi)$	(20) with (10), (12), (16), and (18)
$z_{\eta_{sy}}(\mathcal{R}_c, \eta_{sy})$	(23) and (25)
$z_{\eta\xi_{sy}}(\mathcal{R}_c, \eta_{sy}, \xi_{sy})$	(35) with (23), (25), (29), (32), and (33)

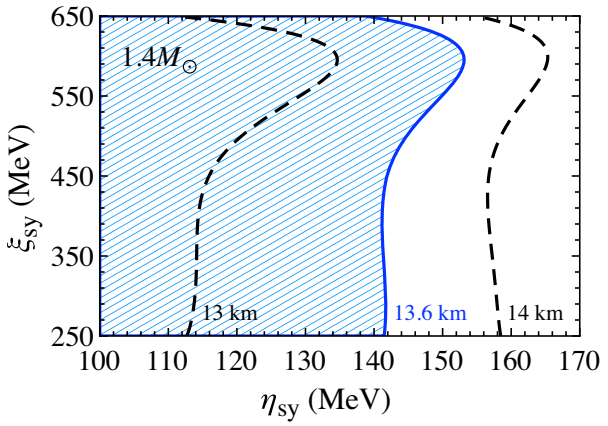

FIG. 13. Constraint on the parameter space with η_{sy} and ξ_{sy} obtained from the constraint on the 1.4 $M_\odot$ neutron star radius $R_{1.4}$, with the gravitational wave event GW1708107, i.e., $R_{1.4} \leq$ 13.6 km [16]. In this figure, the shaded region corresponds to the allowed region.

Finally, in Table VI, we show the corresponding equations for the empirical relations obtained in this study. In addition, using the estimation of the neutron star mass and radius with the empirical formulas $M_{\eta\xi_{sy}}(\mathcal{R}_c, \eta_{sy}, \xi_{sy})$ and $z_{\eta\xi_{sy}}(\mathcal{R}_c, \eta_{sy}, \xi_{sy})$, we make a constraint on the parameter space with η_{sy} and ξ_{sy}. That is, owing to the gravitational wave observations at the GW170817, the tidal deformability of the neutron star has been constrained, which tells us that the $1.4\,M_\odot$ neutron star radius should be less than 13.6 km [16]. In practice, assuming that $M = 1.4\,M_\odot$ together with $M_{\eta\xi_{sy}}(\mathcal{R}_c, \eta_{sy}, \xi_{sy})$ and $z_{\eta\xi_{sy}}(\mathcal{R}_c, \eta_{sy}, \xi_{sy})$, one can estimate the stellar radius with the given values of η_{sy} and ξ_{sy}. In Fig. 13, we plot the combination of η_{sy} and ξ_{sy} so that the radius becomes 13 and 14 km with dashed lines and 13.6 km with the solid line. So, one can see that the shaded region corresponds to the allowed region, considering the constraint through the GW170817.

IV. CONCLUSION

The neutron star mass and radius are one of the most important observables to constrain the EOS for dense matter. In fact, some astronomical observations could make a constraint on EOS, essentially for a higher density region. On the other hand, the terrestrial nuclear experiments constrain the nuclear properties especially around the nuclear saturation density, which enables us to screen the EOSs. So, at least the neutron star models for a lower density region are strongly associated with the nuclear saturation parameters. In this study, we propose the empirical formulas for the neutron star mass and gravitational redshift as a function of the central density and the suitable combination of nuclear saturation parameters, which are applicable to the stellar models constructed with the central density up to threefold nuclear density. Combining both empirical relations, the stellar radius is also estimated. Our empirical formulas can directly connect the neutron star properties to the nuclear saturation parameters, which helps us to imagine the neutron star mass and radius with the specific values of saturation parameters constrained via experiments, and vise versa. As an application with our empirical formulas, we constrain the parameter space of the nuclear saturation parameters, considering the constraint on the neutron star radius through the gravitational wave observations at the GW170817. Although the current constraint is still poor, one can discuss the more severe nuclear saturation parameters with additional future astronomical observations. In this study, we focus only on the empirical relations for the neutron star mass and gravitational redshift, but it must be also possible to derive the empirical formulas for the other neutron star bulk properties, such as moment of inertia or Love number, as in Ref. [46]. We will consider these topics somewhere in the future.

ACKNOWLEDGMENTS

This work is supported in part by Japan Society for the Promotion of Science (JSPS) KAKENHI Grants No. JP18K13551, No. JP19KK0354, No. JP20H04753, and No. JP21H01088 and by Pioneering Program of RIKEN for Evolution of Matter in the Universe (r-EMU).

[1] P. Demorest, T. Pennucci, S. Ransom, M. Roberts, and J. Hessels, Nature (London) **467**, 1081 (2010).
[2] J. Antoniadis *et al.*, Science **340**, 6131 (2013).
[3] H. T. Cromartie *et al.*, Nat. Astron. **4**, 72 (2020).
[4] E. Fonseca *et al.*, Astrophys. J. **915**, L12 (2021).
[5] K. R. Pechenick, C. Ftaclas, and J. M. Cohen, Astrophys. J. **274**, 846 (1983).
[6] D. A. Leahy and L. Li, Mon. Not. R. Astron. Soc. **277**, 1177 (1995).
[7] J. Poutanen and M. Gierlinski, Mon. Not. R. Astron. Soc. **343**, 1301 (2003).
[8] D. Psaltis and F. Özel, Astrophys. J. **792**, 87 (2014).
[9] H. Sotani and U. Miyamoto, Phys. Rev. D **98**, 044017 (2018); **98**, 103019 (2018).
[10] H. Sotani, Phys. Rev. D **101**, 063013 (2020).
[11] T. E. Riley *et al.*, Astrophys. J. **887**, L21 (2019).
[12] M. C. Miller *et al.*, Astrophys. J. **887**, L24 (2019).
[13] T. E. Riley *et al.*, Astrophys. J. **918**, L27 (2021).
[14] M. C. Miller *et al.*, Astrophys. J. **918**, L28 (2021).
[15] B. P. Abbott *et al.* (LIGO Scientific and the Virgo Collaborations), Phys. Rev. Lett. **119**, 161101 (2017).
[16] E. Annala, T. Gorda, A. Kurkela, and A. Vuorinen, Phys. Rev. Lett. **120**, 172703 (2018).
[17] N. Andersson and K. D. Kokkotas, Phys. Rev. Lett. **77**, 4134 (1996).
[18] N. Andersson and K. D. Kokkotas, Mon. Not. R. Astron. Soc. **299**, 1059 (1998).
[19] H. Sotani, K. Tominaga, and K. I. Maeda, Phys. Rev. D **65**, 024010 (2001).
[20] H. Sotani and T. Harada, Phys. Rev. D **68**, 024019 (2003); H. Sotani, K. Kohri, and T. Harada, Phys. Rev. D **69**, 084008 (2004).
[21] H. Sotani, N. Yasutake, T. Maruyama, and T. Tatsumi, Phys. Rev. D **83**, 024014 (2011).
[22] A. Passamonti and N. Andersson, Mon. Not. R. Astron. Soc. **419**, 638 (2012).
[23] D. D. Doneva, E. Gaertig, K. D. Kokkotas, and C. Krüger, Phys. Rev. D **88**, 044052 (2013).

[24] H. Sotani, Phys. Rev. D **102**, 063023 (2020); **102**, 103021 (2020); **103**, 123015 (2021).
[25] H. Sotani and A. Dohi, Phys. Rev. D **105**, 023007 (2022).
[26] J. Estee *et al.* (SπRIT Collaboration), Phys. Rev. Lett. **126**, 162701 (2021).
[27] B. T. Reed, F. J. Fattoyev, C. J. Horowitz, and J. Piekarewicz, Phys. Rev. Lett. **126**, 172503 (2021).
[28] H. Sotani, K. Iida, K. Oyamatsu, and A. Ohnishi, Prog. Theor. Exp. Phys. **2014**, 051E01 (2014).
[29] K. Oyamatsu and K. Iida, Prog. Theor. Phys. **109**, 631 (2003).
[30] K. Oyamatsu and K. Iida, Phys. Rev. C **75**, 015801 (2007).
[31] B. K. Agrawal, S. Shlomo, and V. Kim Au, Phys. Rev. C **72**, 014310 (2005).
[32] F. Douchin and P. Haensel, Astron. Astrophys. **380**, 151 (2001).
[33] E. Chabanat, Interactions effectives pour des conditions extremes d'isospin, Ph.D. thesis, University Claude Bernard Lyon-I, 1995.
[34] H. S. Köhler, Nucl. Phys. **A258**, 301 (1976).
[35] P.-G. Reinhard and H. Flocard, Nucl. Phys. **A584**, 467 (1995).
[36] L. Bennour, P.-H. Heenen, P. Bonche, J. Dobaczewski, and H. Flocard, Phys. Rev. C **40**, 2834 (1989).
[37] H. Shen, H. Toki, K. Oyamatsu, and K. Sumiyoshi, Nucl. Phys. **A637**, 435 (1998).
[38] H. Togashi, K. Nakazato, Y. Takehara, S. Yamamuro, H. Suzuki, and M. Takano, Nucl. Phys. **A961**, 78 (2017).
[39] M. Oertel, M. Hempel, T. Klähn, and S. Typel, Rev. Mod. Phys. **89**, 015007 (2017).
[40] B. A. Li, P. G. Krastev, D. H. Wen, and N. B. Zhang, Euro. Phys. J. A **55**, 117 (2019).
[41] E. Khan and J. Margueron, Phys. Rev. C **88**, 034319 (2013).
[42] J. M. Lattimer and Y. Lim, Astrophys. J. **771**, 51 (2013).
[43] P. Danielewicz and J. Lee, Nucl. Phys. **A818**, 36 (2009).
[44] I. Tews, J. M. Lattimer, A. Ohnishi, and E. E. Kolomeitsev, Astrophys. J. **848**, 105 (2017).
[45] H. Sotani, N. Nishimura, and T. Naito, arXiv:2203.05410.
[46] H. O. Silva, H. Sotani, and E. Berti, Mon. Not. R. Astron. Soc. **459**, 4378 (2016).
[47] H. Sotani, Phys. Rev. C **95**, 025802 (2017).
[48] H. Sotani and K. D. Kokkotas, Phys. Rev. D **95**, 044032 (2017).